Supporting information

Surface confined titania redox couple for ultrafast energy storage

Jian Zhi[a†], Houlei Cui[a†], Zhou Wang[a], Fuqiang Huang[a,b*]

a.   State Key Laboratory of High Performance Ceramics and Superfine Microstructure,

Shanghai Institute of Ceramics, Chinese Academy of Sciences, Shanghai 200050, P. R.

China.

b.   Beijing National Laboratory for Molecular Sciences and State Key Laboratory of

Rare Earth Materials Chemistry and Applications, College of Chemistry and Molecular

Engineering, Peking University, Beijing 100871, P. R. China.

† These authors contributed equally to this work.

*Email: huangfq@mail.sic.ac.cn

Experimental section

Synthesis of B-TNAs

The highly ordered TNAs were prepared on Ti foil (99.5% purity, 250 μm in thickness, Alfa Aesar) via a two-step electrochemical anodization process with copper plate as cathode. The employed electrolyte was 0.4 wt% NH_4F in a mixture of glycol and water (97:3 in volume). Ti foil was first anodized at 100 V supplied by a DC power supply for 25 minutes. Second step of anodization process was carried out in the same electrolyte at 100 V for another 25 mins to obtain high-quality TNAs. After dried in air, the as-prepared TNAs (denoted as As-TNAs) were heated at 500 °C for 8 hours in air (obtaining TNAs), or in Al-reduction device (obtaining B-TNAs), respectively. When conducting Al-reduction process, As-TNAs samples and Al powder were separately placed in a special designed two-zone tube furnace and then evacuated to vacuum. Subsequently, As-TNAs and Al powder were annealed at 400 °C and 550 °C respectively and kept for 8 hours. By prolonging the anodizing time to 50 minutes at the second step, B-TNAs with much larger surface area (38 m^2 g^{-1}) and tube length (2.5 μm) can be obtained (denoted as LB-TNAs). To determine the mass loading of TNAs based materials on Ti substrate, Ti foil was removed from HCl solution and the residue particles were rinsed with ethanol. The average mass on 1 cm^{-2} Ti foil is about 2.3 mg.

Synthesis of B-TNAs/PANI

B-TNAs/PANI was obtained from depositing polyaniline on B-TNAs substrate in 0.25 M H_2SO_4 and 0.05 M aniline solution at room temperature (300 K) in cyclic voltammetry mode (CHI760B, CH Instruments) through 30 cyclic voltammetric scans

from -0.2 to 0.9 V (versus SCE) at 50 mV s^{-1}. The back and the margin of Al-TNAs substrate was protected from the electrolyte with our homemade device. Subsequent to the deposition, the compound electrode was washed with dilute H_2SO_4 and ethanol to remove the loose PANI particles on the surface. To determine the mass loading of active materials on Ti substrate, Ti foil was removed from HCl solution and the residue particles were rinsed with ethanol and then dried at 60 °C. The average mass of TNAs, B-TNAs, B-TNAS/PANI and B-TNAs/PANI on 1 cm^{-2} Ti foil is about 2.1 mg, 2.0 mg, 2.6 mg, 2.8 mg, respectively.

Characterizations

Field emission scanning electron microscopy was performed on Hitachi S-4800 instrument. Transmission electron microscopy was performed on Philips Tecnai G2 F20. X-ray diffraction was conducted on Bruker D8 Advance. X-ray photoelectron spectroscopy was performed on PHI 5000C ESCA System with Mg Ka X-ray (hv=1253.6 eV) at 14 kV. Raman spectroscopy was investigated on Renishaw InVia Reflex with 532 nm laser excitation. The electrical conductivities of various TNAs samples were investigated using an Accent HL5500 Hall System. As B-TNAs were grown on Ti foil, we cannot differentiate the conductivity of B-TNAs from the measured value of TiO_2/Ti composites due to the impact of Ti metal. Therefore, carefully scratching B-TNAs powders from Ti foil and pressing them into pellets is an effortless way to get the conductivity of pristine material on Ti substrate. To collect enough oxide powders for conductivity measurement, several pieces of large area (2

cm × 2 cm) Ti foils were anodized and submitted to Al-reduction (and PANI skinning for B-TNAs/PANI sample) using the same method.

Preparation of B-TNAs with other methods

NaBH$_4$ reduction:[1] As prepared TNAs were dipped in 0.1 M NaBH4 for 40 at room temperature followed by rinsing with water and air drying. Gray colored TNAs were obtained after this treatment.

Ambient hydrogen gas treatment:[2] Hydrogenation was performed under a H$_2$ gas flow (50 sccm) at atmospheric pressure while as prepared TNAs were placed in a quartz tube maintained at an elevated temperature in the range of 500°C. A successive hydrogenation for 30 min was performed on aTiO2, resulting in a gradual color change from white to gray.

Hydrogen plasma treatment:[3] As prepared TNAs was placed in a thermal plasma furnace by hydrogen plasma for 4 h at 500 ° C. The plasma input power was 200 W. The obtained B-TNAs via this method is dark-brown.

Electrochemical anodizing:[4] The electrochemical reduction processes were conducted in a typical three-electrode system, with the TNAs electrode, Ag/AgCl electrode, and Pt mesh as working electrode, reference electrode, and counter electrode, respectively. In this step, the TNAs underwent electrochemical reduction under negative potential (−0.4 V vs. reversible hydrogen electrode (RHE)) in the supporting electrolyte of 1 M Na$_2$SO$_4$ for 30 min. The obtained grey colored sample was finally cleaned with DI water and dried off with N$_2$ gas.

Electrochemical Characterizations

To characterize the supercapacitor performance of the samples, a conventional three-electrode system was utilized to conduct electrochemical measurements. The TNAs attached on Ti substrates were used directly as the working electrode, with a Pt wire and an Ag/AgCl (KCl saturated) electrode as counter and reference electrodes respectively in 1 M H_2SO_4 aqueous solution. Electrochemical impedance spectroscopy (EIS), cyclic voltammetry (CV) and galvanostatic charge-discharge (GCD) tests were carried out by Biologic-VMP3 electrochemical workstation. Mott-Schottky plots were derived from impedance-potential tests conducted at a frequency of 1 kHz in the dark, and Nyquist plots were acquired from AC impedance tests performed over a frequency range of 0.01 Hz to 100 kHz at an amplitude of 5 mV. The cycling stability was tested by CV measurements at a constant scan rate of 100 mV s^{-1} for 2000 cycles.

The B-TNAs/PANI//MG asymmetric supercapacitor device was assembled by separating the positive and negative electrodes with a NKK separator (Nippon Kodoshi Corporation, 0.03 mm). MG was synthesized according to our previous report. [5] The mass ratio of active materials in positive and negative electrodes is 0.38 (determined by the specific capacitance of MG and B-TNAs/PANI). Total mass of active materials is 10.2 mg, containing 2.8 mg B-TNAs/PANI on Ti foil as positive electrode, 7.4 mg MG as negative electrode.

B-TNAs and B-TNAs/PANI symmetric cells using 1-butyl-3-methylimidazolium tetrafluoro-borate ($BMIMBF_4$)/acetonitrile (AN) or tetraethyl ammonium tetrafluoroborate ($TEABF_4$)/ propylene carbonate (PC) were assembled in glove box.

The LiBs characterization was performed using 2032-type coin cells with two electrodes, assembled in an Ar-filled dry glove box using TNAs based material (TNAs/PANI and B-TNAs/PANI) on Ti-foil and Li metal as the working electrode and counter electrode, respectively. 1M $LiPF_6$ in ethyl carbonate (EC)/dimethyl carbonate (DMC) (3/7 by volume) was used as an electrolyte and two pieces of porous 25 μm thick polypropylene were used as separators. The discharge-charge cycling was performed between 0-3 V (vs. Li/Li$^+$) at room temperature, using different C-rates on a battery tester (Neware) (1 C=335 mA/g). Cyclic voltammetry (CV) testing was performed between 0.01 and 3 V (vs Li/Li$^+$) with a scan rate of 0.1 mV s^{-1}. In the full cell, the mass loading of $LiMn_2O_4$ is slightly smaller than TNAs based materials in the anode, and the specific capacity is calculated based on the mass of $LiMn_2O_4$. A glass fiber from Whatman was used as a separator. The electrolyte consisted of a solution of 1 M $LiPF_6$ in ethylene carbonate/dimethyl carbonate/diethyl carbonate (1:1:1, in wt %) obtained from Tianjin Jinniu Power Sources Material Co., Ltd. Galvanostatic cycling tests of the assembled cells were carried out on an Arbin BT2000 system in the voltage range of 1−2.5 V.

To simulate the performance of B-TNAs based electrode in grid-scale application, Hybrid battery, the combination of a Li-ion full cell and an asymmetric supercapacitor, was fabricated.[6] The testing platform of a hybrid battery is mainly constructed by a digital oscilloscope, a function generator, and a voltage/current (V/C) converter. The V/C converter is composed by an operational amplifier (OPA), a Metal-Oxide-Semiconductor Field-Effect Transistor (MOSFET) and a current set resistor.[7]

First, the function generator is to produce a sinusoidal-wave signal $V_S(t)$ shown as:

$$V_s(t) = V_m + V_m sin2\pi ft \quad (1)$$

where V_m is the peak voltage of $V_S(t)$, and f is the charging frequency. Then the sinusoidal-wave signal $V_S(t)$ is sent to the V/C converter to produce the charging current $I_C(t)$, and the corresponding sinewave impedance can be obtained through below calculation:

$$R_s(t) = \frac{V_s(t)}{I_c(t)} = \frac{V_m + V_m sin2\pi ft}{I_c(t)} \quad (2)$$

In comparison, PbO_2 based hybrid battery was assembled merging a valve-regulated lead–acid cell with an asymmetric PbO_2/activated carbon supercapacitor. [6]

Calculations of capacitance:

The areal capacitance in three-electrode cell was calculated from CV curves according to equation (3):

$$C_a = \frac{\int dV}{2\mu\Delta VS} \quad (3)$$

where I is the voltammetric current, V is the potential in one sweep segment, ν is the potential scan rate, ΔV is the potential window, S is the surface area of working electrode.

The specific capacitance (C_s) of one electrode in symmetrical cell is shown in equation (4):

$$C_s = \frac{2I\Delta t}{S_0\Delta V} \quad (4)$$

Where S_0 is the area of one electrode, Δt is the time for a full discharge and ΔV is the potential change after a full discharge.

The specific capacitance derived from galvanostatic discharge curves of the whole asymmetric devices was calculated based on equation (5):

$$C_{as} = \frac{I\Delta t}{S\Delta V} \quad (5)$$

in which I is the discharge current, S is the total surface area on the two electrodes, Δt is the time for a full discharge and ΔV is the potential change after a full discharge. The energy density (E) and power density (P) of the device depicted in the Ragone plots were calculated by employing the equations (6) and (7):

$$E = \frac{1}{2}C\Delta V^2 \quad (6)$$

$$P = \frac{E}{t} \quad (7)$$

in which C is the specific capacitance, ΔV is the potential window after IR drop, t is the discharging time and m is the total mass of active materials on the two electrodes.

Calculations of Li$^+$ diffusivity of TNAs/PANI and B-TNAs/PANI based on EIS data:

EIS results of these two samples are fitted using an equivalent circuit. In the equivalent circuit, R_s indicates the ohmic resistance of electrolyte and electrode; R_{ct} is attributed to the charge-transfer resistance at the active material interface; CPE represents the double-layer capacitance and passivation film capacitance. W is the Warburg impedance caused by a semi-infinite diffusion of Li+ ion in the electrode. Z_{re} from EIS is highly related to the root square of the lower angular frequencies. Through linear fitting, the Warburg impedance coefficient (σ_w) can be obtained from the straight lines. The relation is governed by equation (8):

$$Z_{re} = R_s + R_{ct} + \sigma_w \omega - 1/2 \qquad (8)$$

where R_{ct}: charge-transfer resistance, Rs: ohmic resistance and ω: angular frequency in the low frequency region. After obtaining σ_w, the diffusivity values of the lithium ions diffusing into the electrode materials can be further calculated using equation (9):

$$D_{Li} = 0.5 \left(\frac{RT}{AF^2 \sigma_w C} \right)^2 \qquad (9)$$

D_{Li}: Li$^+$ diffusivity, R: the gas constant, T: the absolute temperature, F: Faraday's constant, A: the contact area between active materials and electrolyte (here the geometric area of electrode) and C: molar concentration of Li$^+$ ions.

In this study, williamson–Hall analysis of (001) peaks of XRD data in TNAs/PANI and B-TNAs/PANI before and after cycling was conducted to quantify the impact of microstrain. β_{inst}, stands for the instrumental broadening, was used as correction factor to regulate (00l) peak of TiO_2 using equation (10):

$$\beta_{hkl} = \sqrt{{\beta'_{hkl}}^2 - {\beta_{inst}}^2} \qquad (10)$$

Here β'_{hkl} represents the observed halfway-full-width of (001) peak. After calculating β_{hkl}, the microstrain (ε) can be calculated using equation (11):

$$\varepsilon = \frac{\beta_{hkl}}{4 \tan\theta} \qquad (11)$$
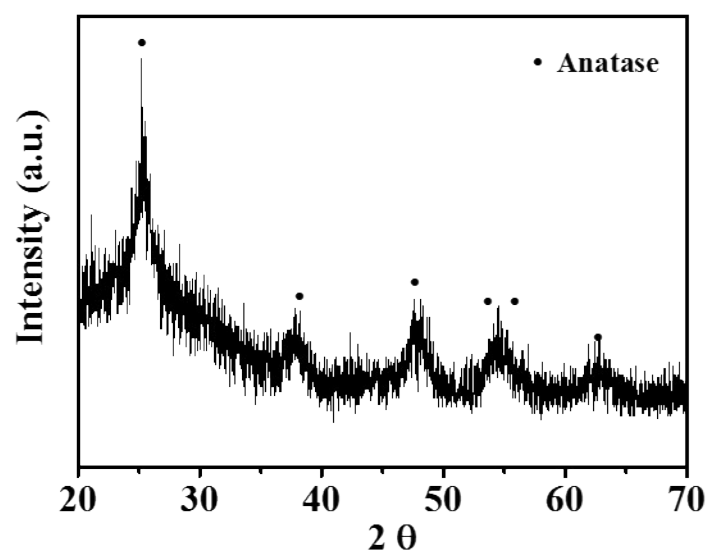
Figure S1: XRD patterns of B-TNAs.
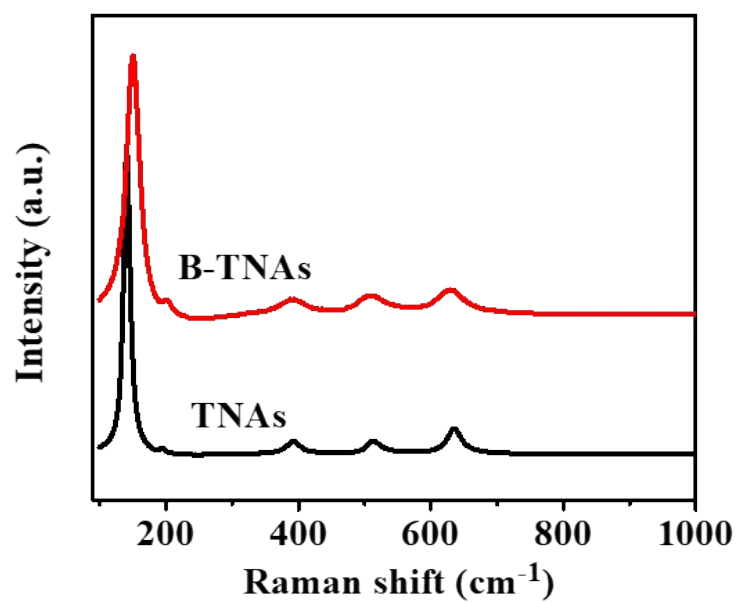
Figure S2. Raman spectra of B-TNAs and TNAs.
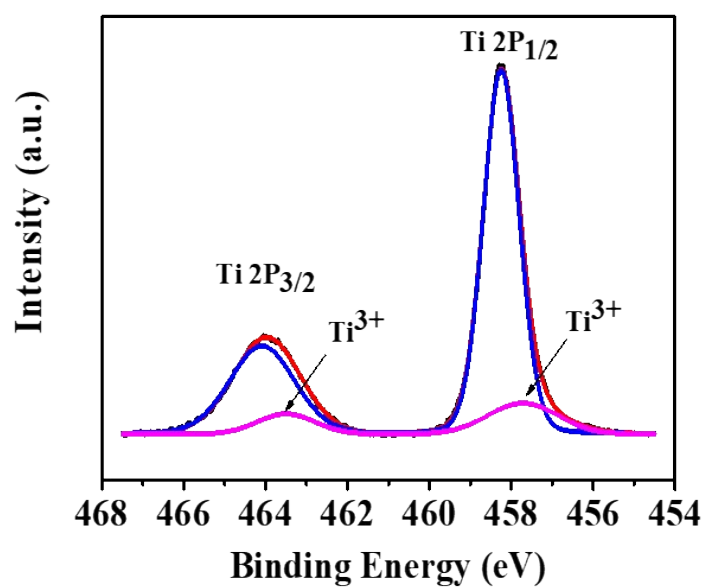
Figure S3. Ti 2p XPS spectra of B-TNAs.
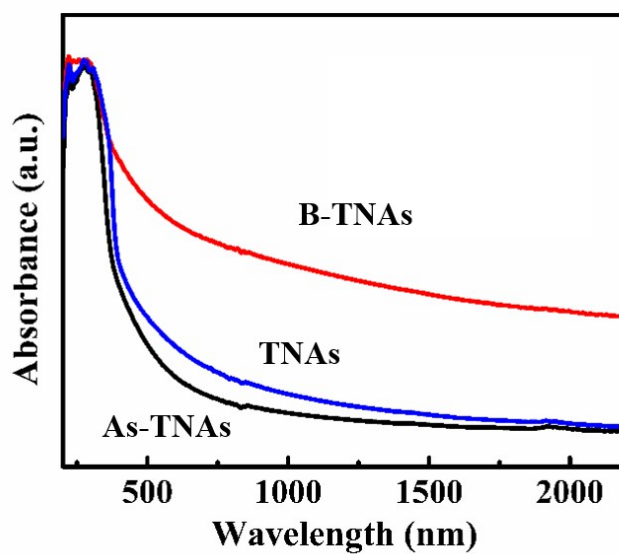
Figure S4. Absorption spectra of TNAs after anodization (denoted as As-TNAs), TNAs, and B-TNAs, measured by coating exfoliated and dispersed TNAs on Quartz glass.
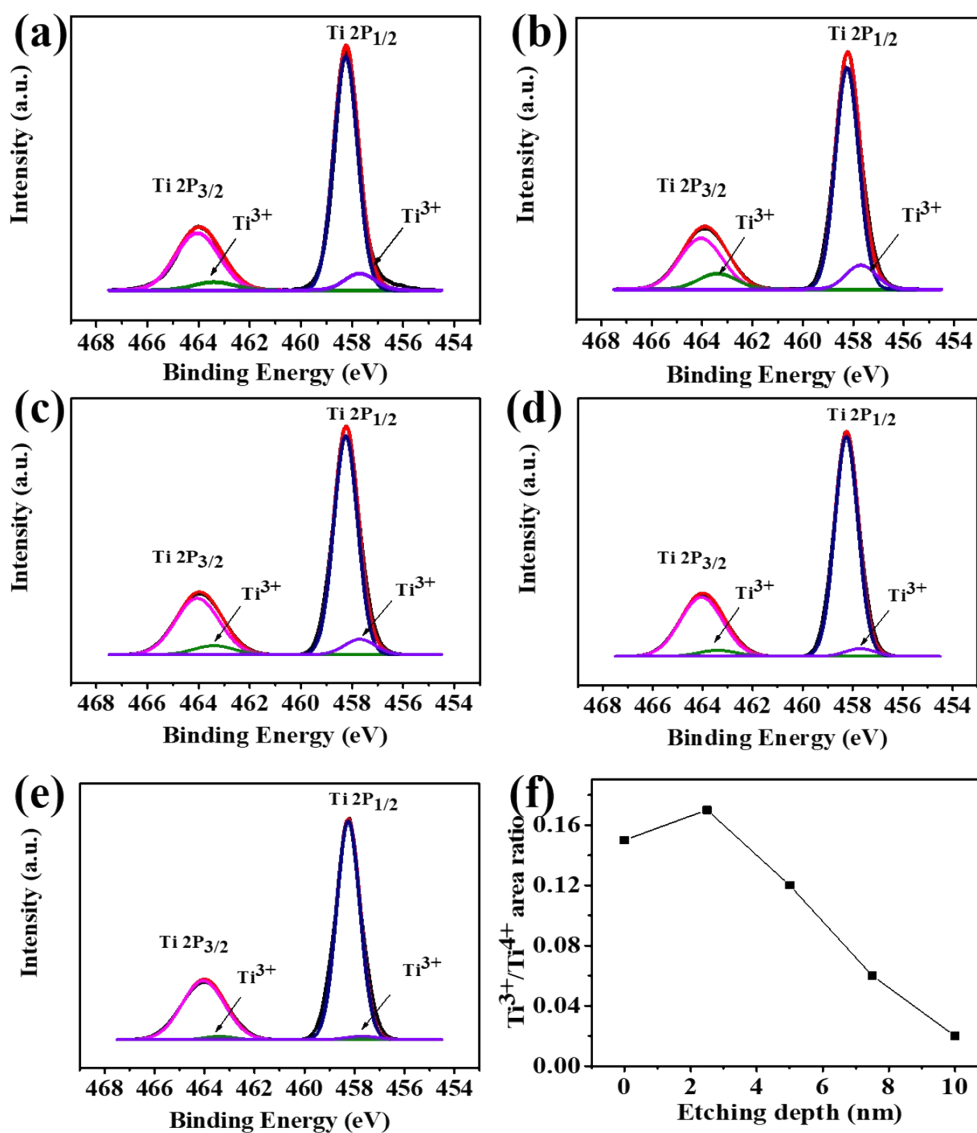
Figure S5. Ti 2p XPS spectra of B-TNAs with different etching time: (a) 0 minute; (b) 5 minutes; (c) 10 minutes; (d) 15 minutes; (e) 20 minutes. (f) $[Ti^{3+}]/[Ti^{4+}]$ area ratio from XPS spectra as a function of etching depth.
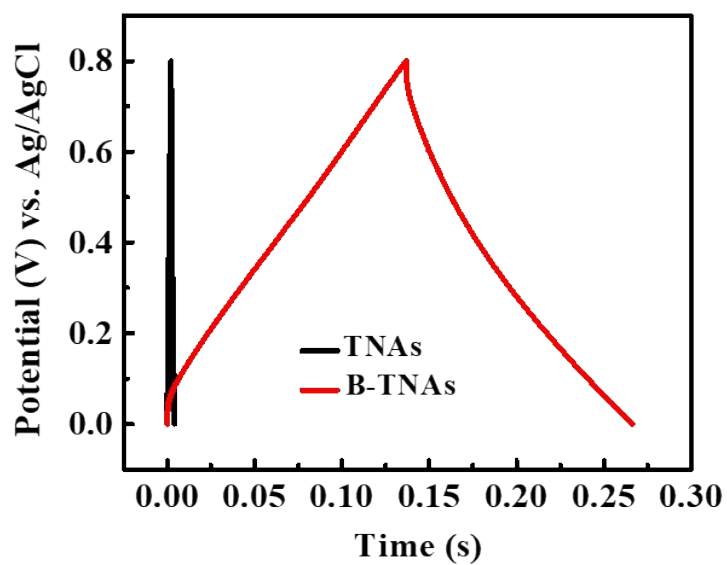
Figure S6. Charge/discharge curves of TNAs and B-TNAs at a current density of 400

mA cm^{-2}.
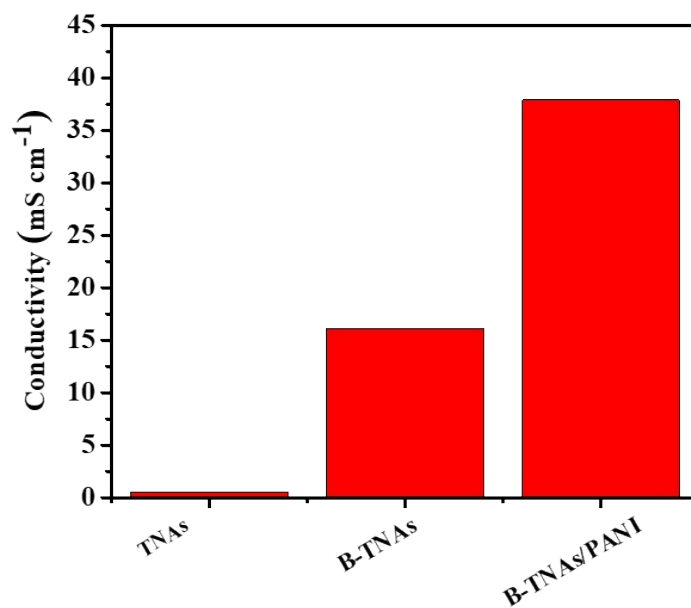
Figure S7. Electrical conductivity of the pressed pellets of TNAs, B-TNAs and B-TNAs/PANI.
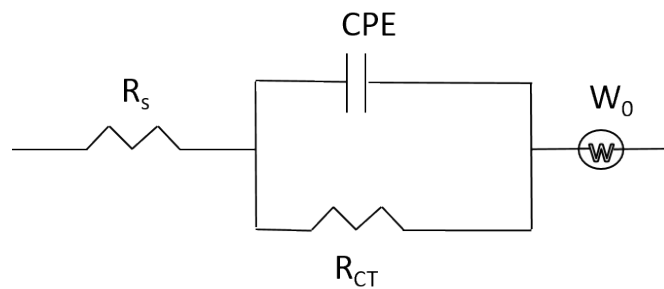
Figure S8. Corresponding equivalent circuit in Figure 2d.
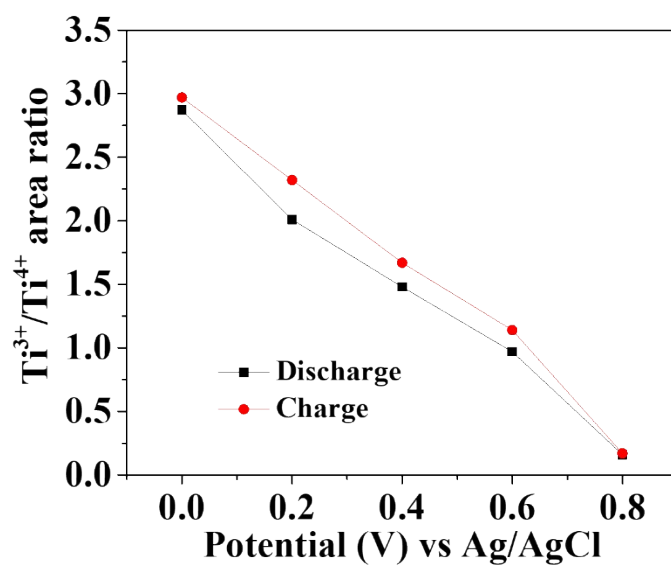
Figure S9. The peak area ratio from Ti^{3+}/Ti^{4+} as a function of applied potential during the electrochemical redox cycle of B-TNAs electrode.
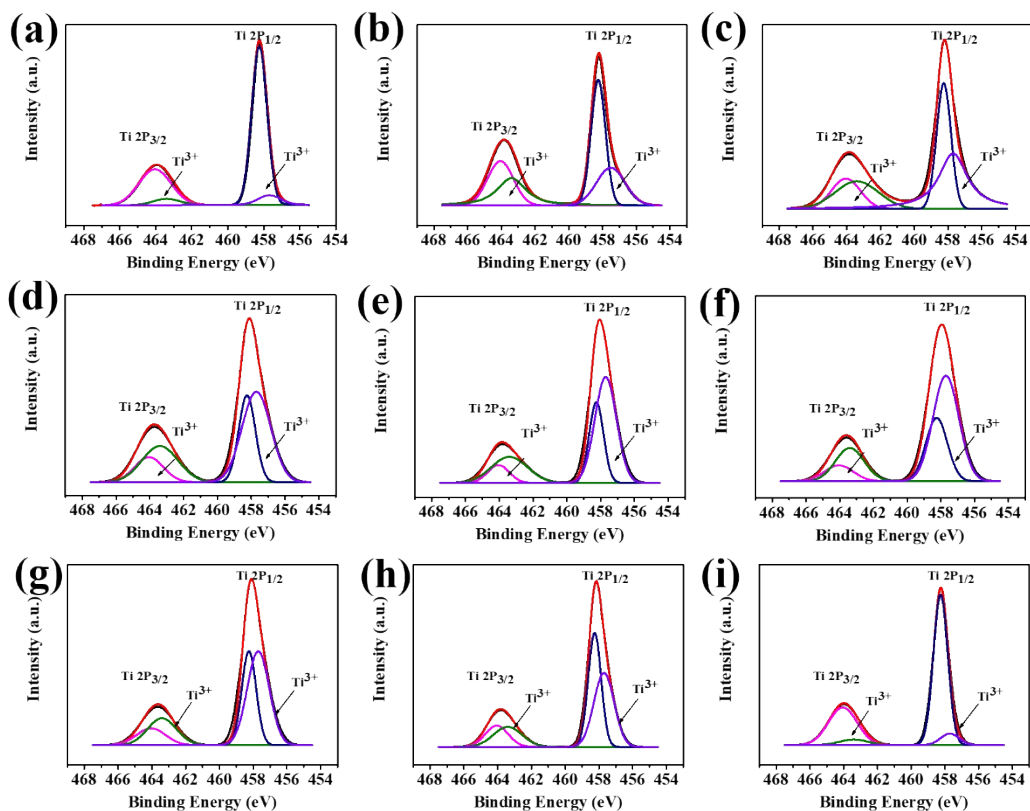
Figure S10. XPS spectra corresponding to Figure S9, where Figure S10(a-e) represents the discharge of B-TNAs from 0.8-0V and Figure S10(f-i) relates to the charge of B-TNAs back to 0.8V.
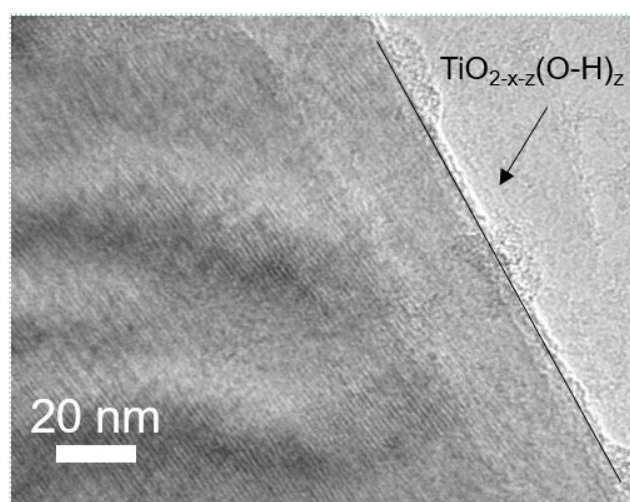
Figure S11. Ex-situ high resolution TEM image of B-TNAs after fully discharged.
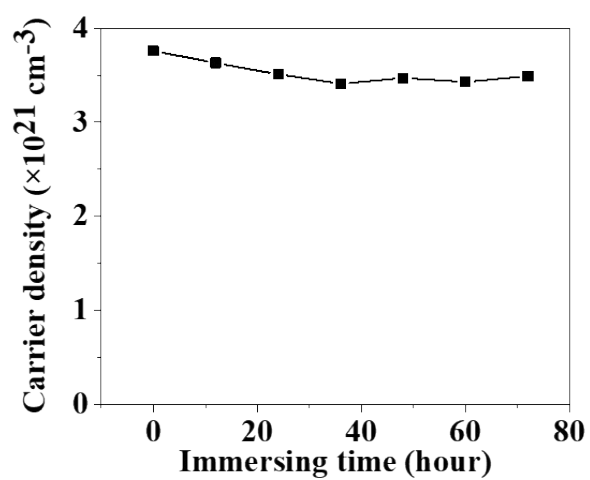
Figure S12. Calculated carrier densities of B-TNAs as a function of time immersing

in 1M H_2SO_4 electrolyte.
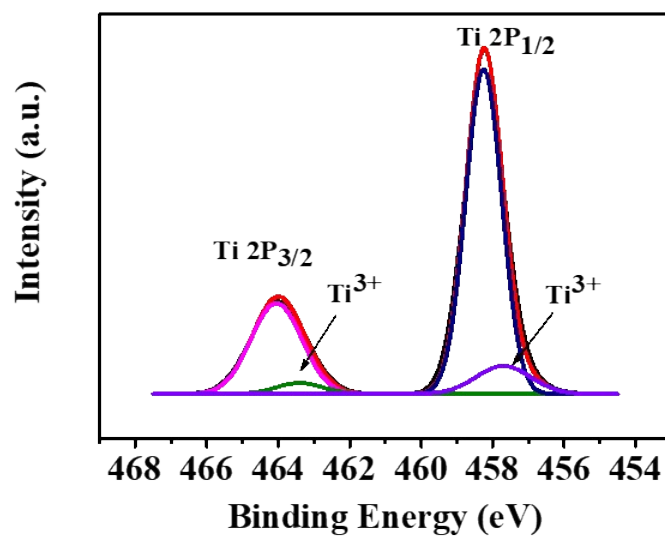
Figure S13. XPS pattern of B-TNAs after acid immersing for 72 hours.
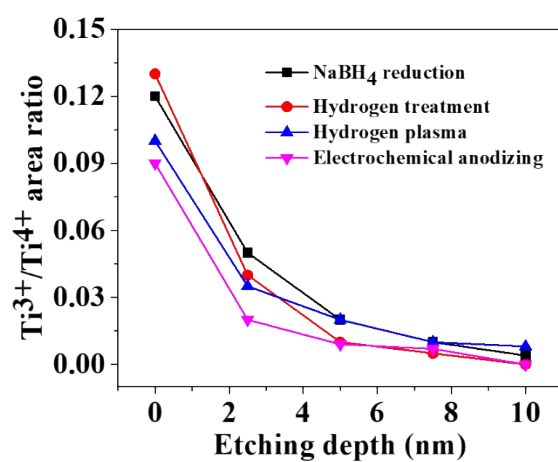
Figure S14. evolution of the $[Ti^{3+}/Ti^{4+}]$ area ratio from XPS spectra as a function of depth in B-TNAs samples prepared from $NaBH_4$ reduction, ambient hydrogen treatment, hydrogen plasma and electrochemical anodizing.
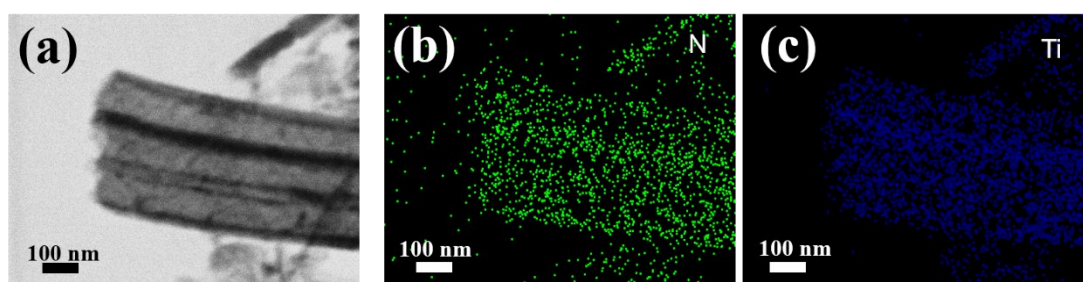
Figure S15. Energy-dispersive X-ray spectrometry (EDX) mapping analysis (N,Ti) for B-TNAs/PANI.
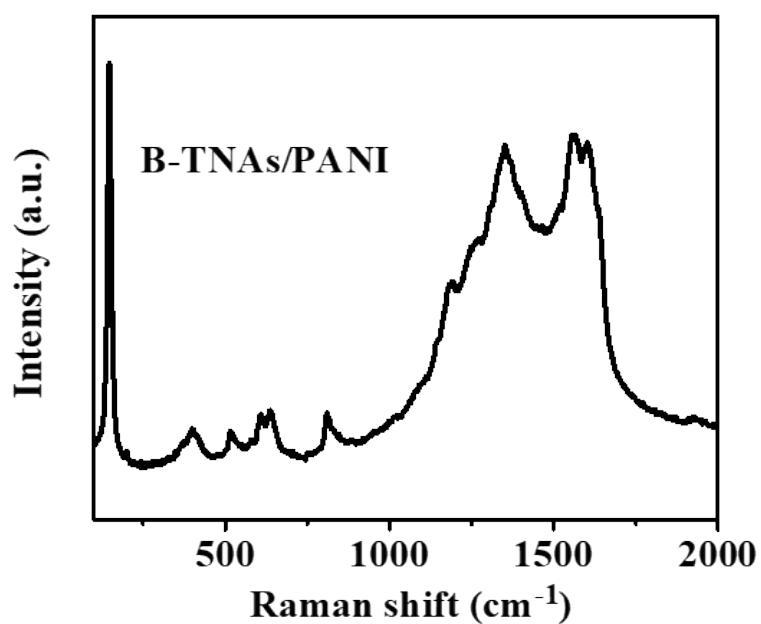
Figure S16. Raman spectra of B-TNAs/PANI. After electrochemical polymerization, the C-C deformation bands of the benzoid ring can be found at 1600 and 1563 cm^{-1} in the Raman spectra of B-TNAs/PANI (Figure S11), indicating the formation of PANI.[8] The peaks at 1405 and 1347 cm^{-1} are due to C–N stretching of delocalized polaronic charge carriers. The benzene C-H bending deformation band at 1179 cm^{-1} is characteristic of the reduced and semiquinone structures.[9]
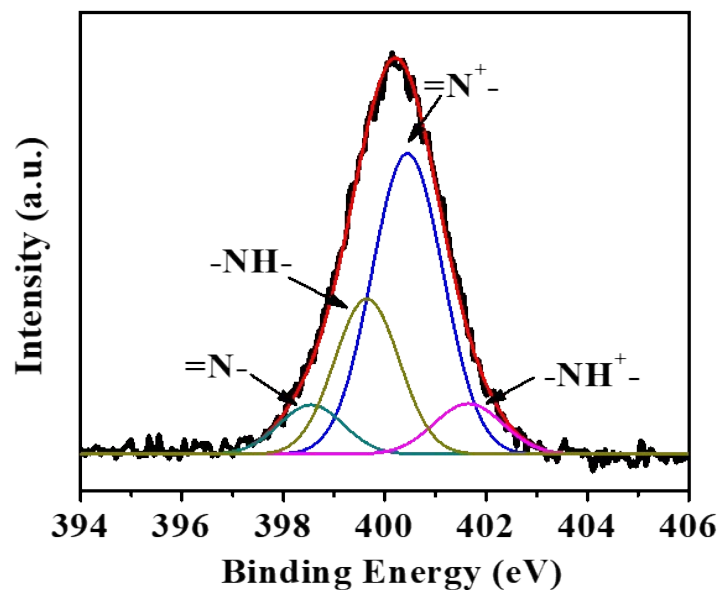
Figure S17. N 1s XPS spectra of B-TNAs/PANI. The spectra is deconvoluted to four

Gaussian peaks at the binding energy of 397.9, 398.8, 400.9 and 401.7 eV. These peaks

are belonged to imine-like structure [=N-], amine-like nitrogen atoms [-NH-],

protonated imine [=N$^+$-], and protonated amine [-NH$^+$-], respectively, corroborating the
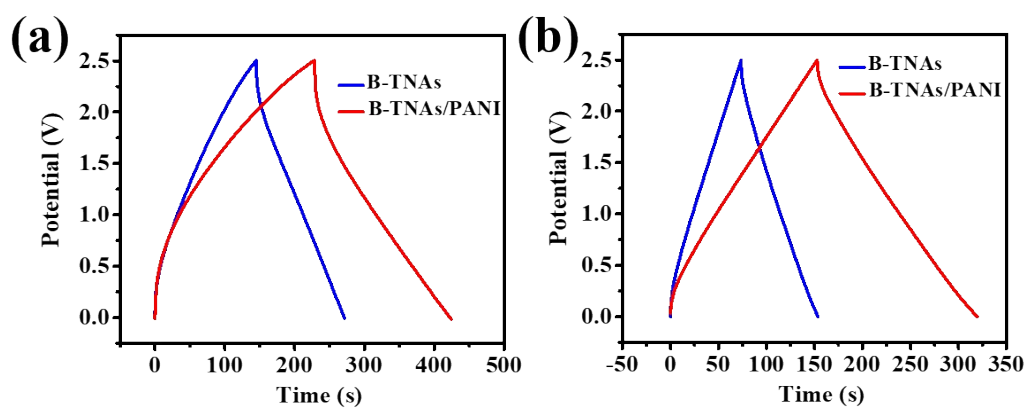
PANI deposition on B-TNAs.
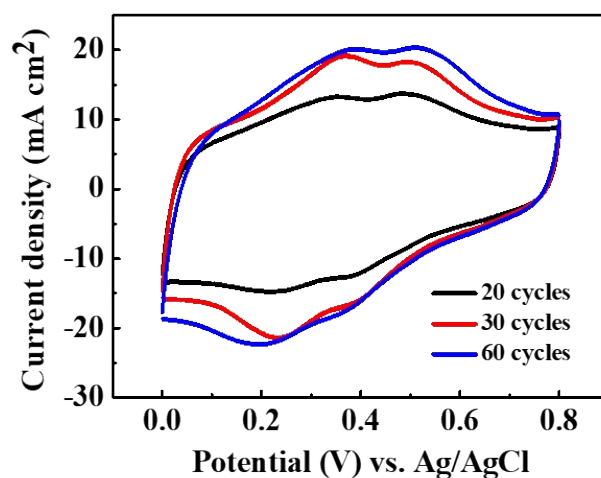
**Figure S18**. CV curves of B-TNAs/PANI obtained at different scan numbers.
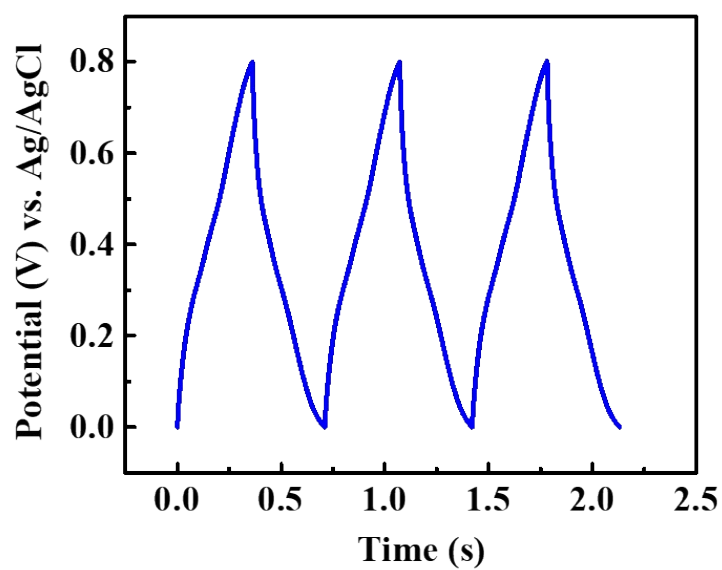
Figure S19. Charge/discharge curves of B-TNAs/PANI at a current density of 400
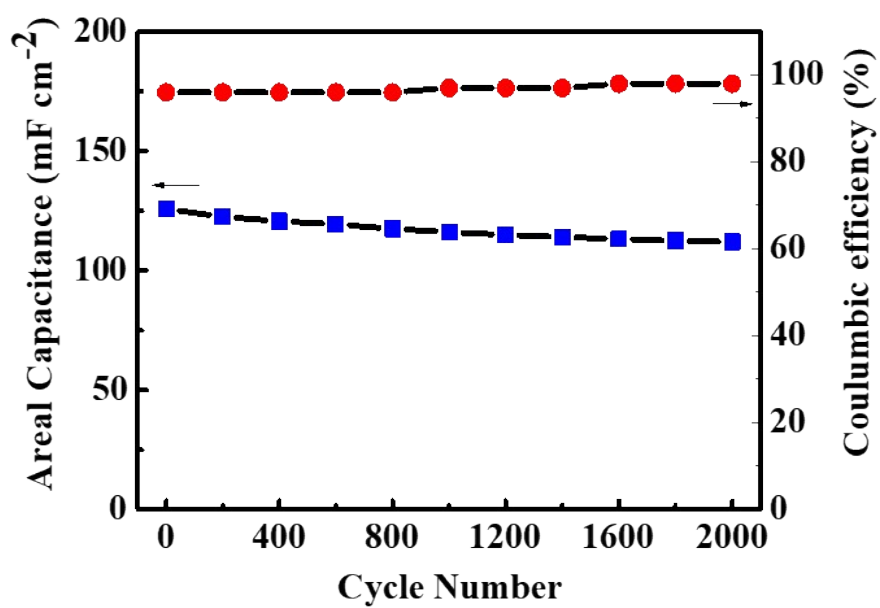
mA cm^{-2}.

**Figure S20**. Cycle life and corresponding coulombic efficiency of B-TNAs/PANI.

Figure S21. Charge/discharge curves of symmetric supercapacitor employing B-TNAs or B-TNAs/PANI as electrodes under a current density of 0.5 mA cm^{-2}: (a) Symmetric cell in 1M BMIMBF$_4$/AN electrolyte; (b) Symmetric cell in 1M TEABF$_4$/PC electrolyte.
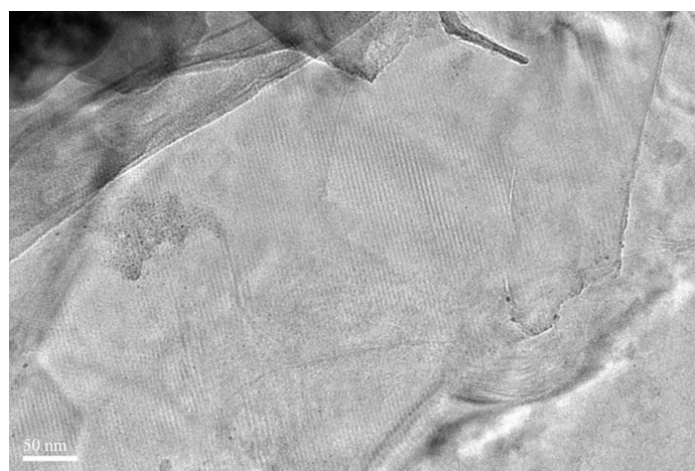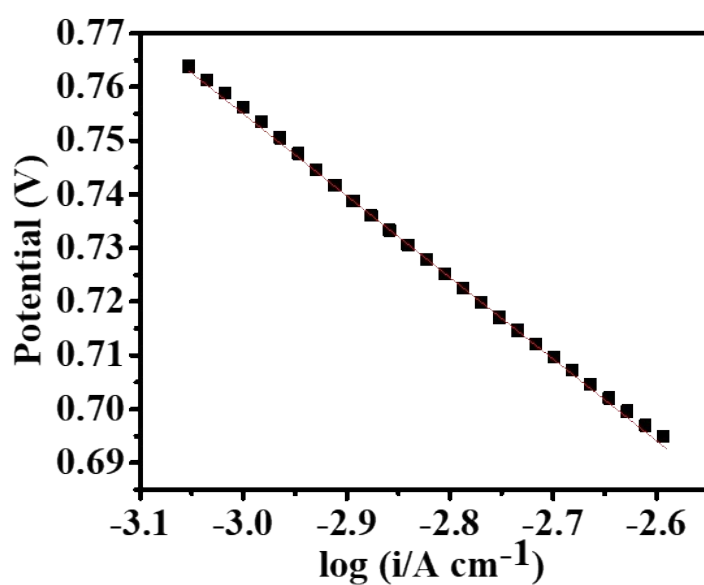

**Figure S22.** TEM image of mesoporous graphene (MG).
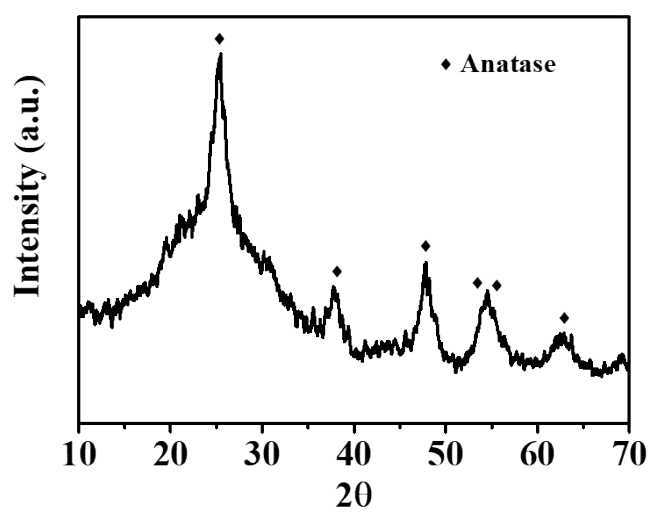
Figure S23. XRD pattern of B-TNAs/PANI after 10000 cycles in asymmetric supercapacitor cell.
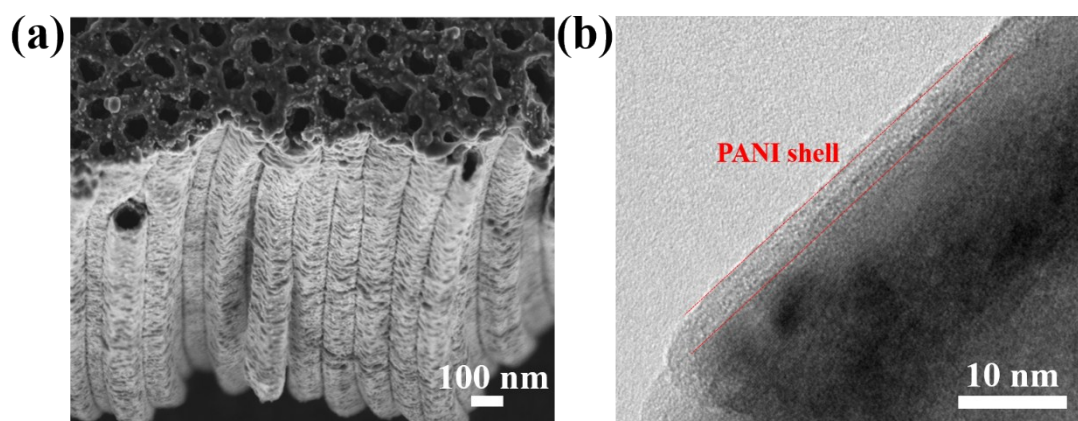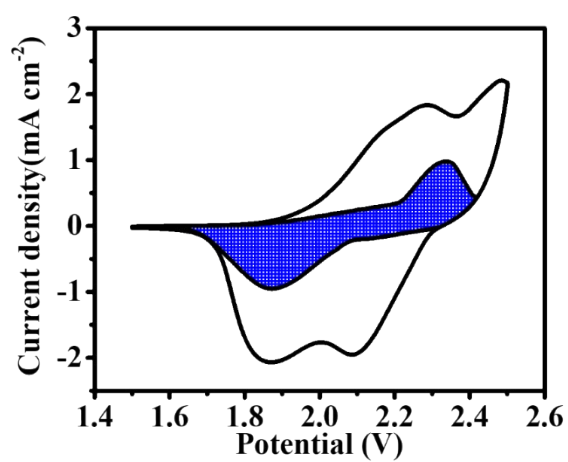

Figure S24. (a,b) High resolution SEM and TEM images of B-TNAs/PANI after 10000 cycles.
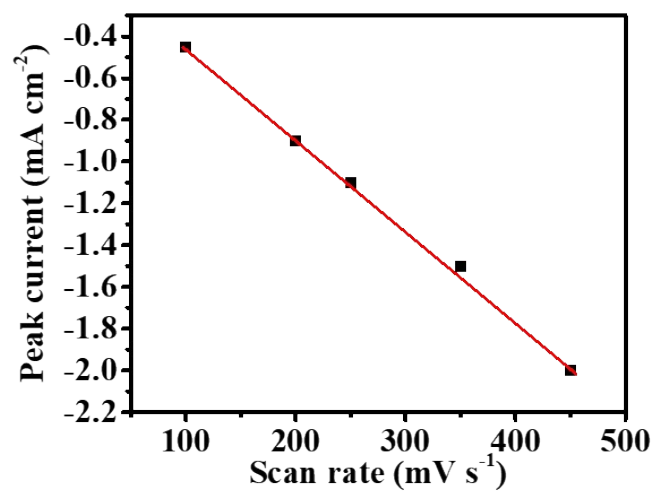
Figure S25. Electrode potential of B-TNAs as a function of current density at Tafel

zone characterized in 1M LiPF$_6$/ethyl carbonate (EC)/dimethyl carbonate (DMC)

electrolyte.
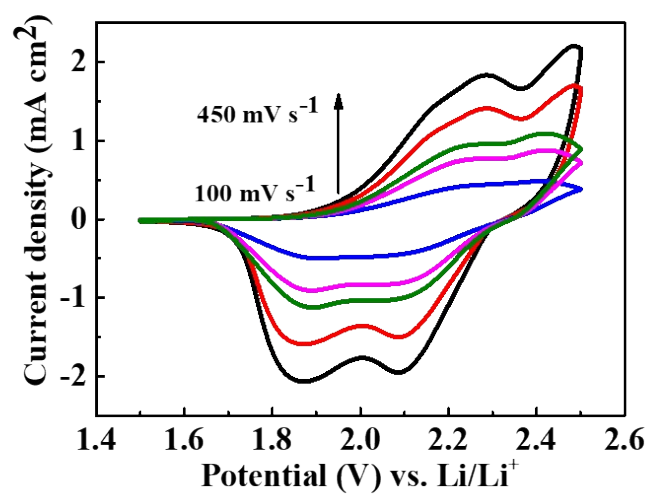
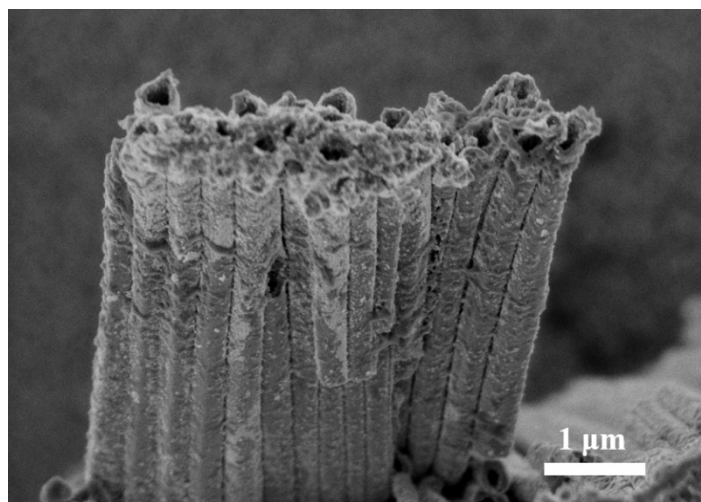**Figure S26**. CV curves of B-TNAs/PANI obtained at different scan rates.

Figure S27. Capacitive contributions (shaded area) to the total current for B-

TNAs/PANI electrode at 0.35 V s^{-1}.

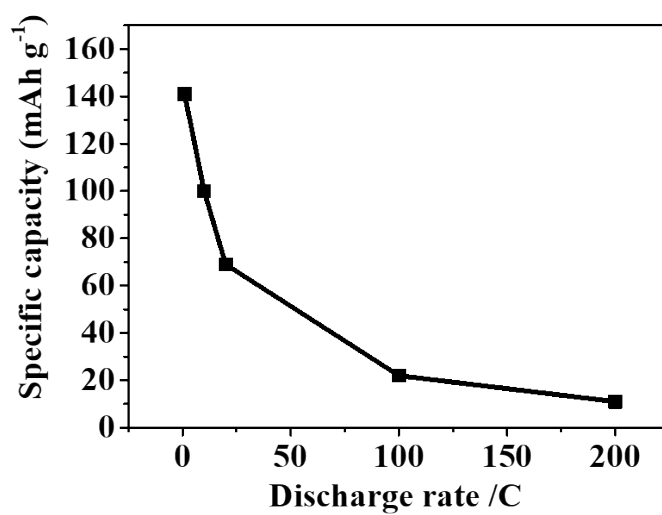**Figure S28**. The relationships between the peak current of B-TNAs/PANI at 1.86V
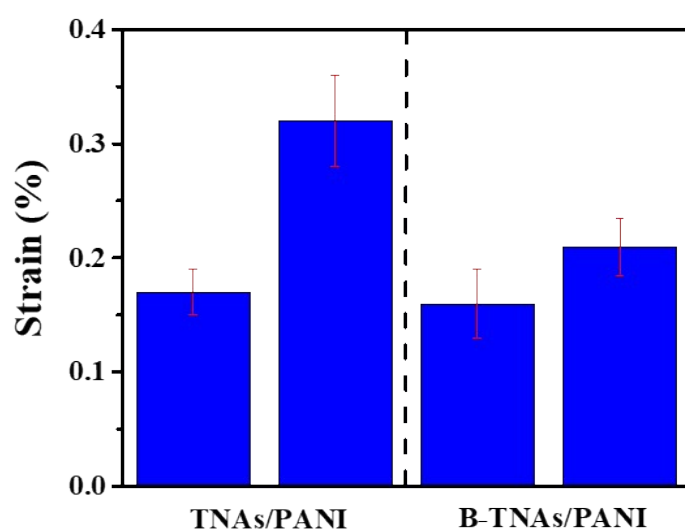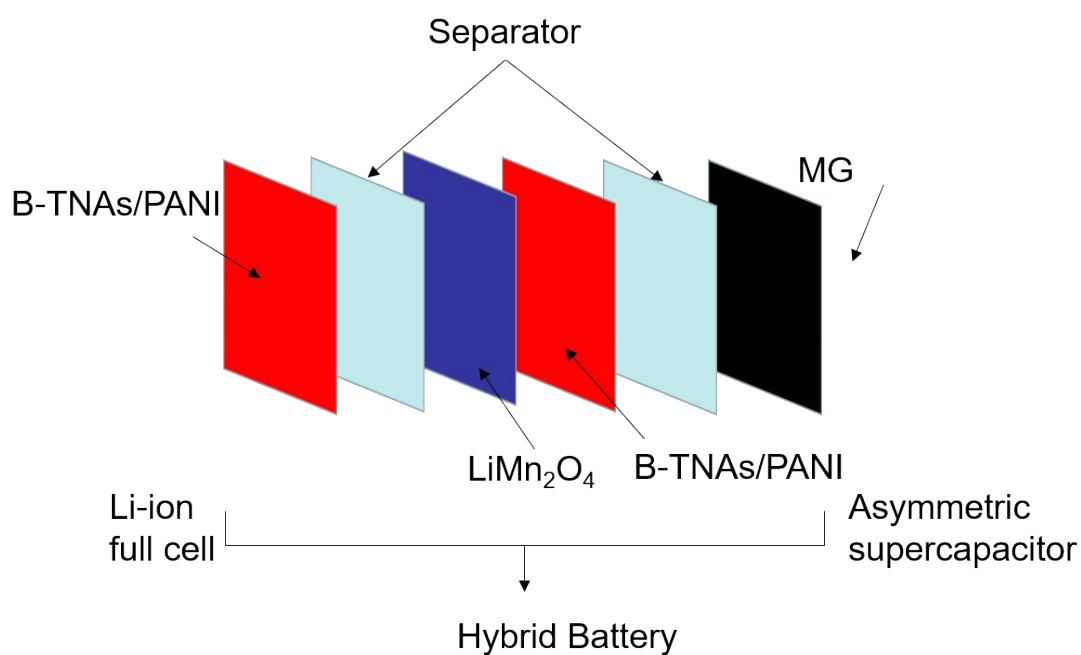
and scan rate.

Figure S29. SEM image of LB-TNAs

Figure S30. The rate capability at different current densities from 1C to 200 C of

half-cells employing LB-TNAs.

Figure S31. Comparison of microstrain, before (left) and after (right) extensive cycling for 2000 cycles for TNAs/PANI and B-TNAs/PANI based half-cells.

Figure S32. Configuration of a hybrid battery

Table S1. Electrochemical properties of B-TNAs prepared by various methods

Methods	carrier densities (cm^{-3}) [a]	Conductivity (mS cm^{-1}) [b]	Areal capacitance (mF cm^{-2}) [c]
NaBH$_4$ reduction	2.58×10^{19}	1.2	18
Ambient hydrogen treatment	5.76×10^{20}	4.6	27

Hydrogen plasma	9.43×10^{20}	5.3	36
Electrochemical anodizing	6.32×10^{19}	1.7	22
Aluminum reduction	3.76×10^{21}	16.1	71

[a] Calculated from Mott-Schottky plots. Note that in all cases only surface of TiO_2 are reduced, the carrier densities can be direct indicative of surface conductivity.

[b] After etching Ti substrates by HCl solution.

[c] At a scan rate of 5 mVs^{-1}, in three-electrode cell.

References

[1]   Q. Kang, J. Cao, Y. Zhang, L. Liu, H. Xu, J. Ye, *Journal of Materials Chemistry A* **2013**, 1, 5766.

[2]   X. Yu, B. Kim, Y. K. Kim, *ACS Catalysis* **2013**, 3, 2479.

[3]   Z. Wang, C. Yang, T. Lin, H. Yin, P. Chen, D. Wan, F. Xu, F. Huang, J. Lin, X. Xie, *Advanced Functional Materials* **2013**, 23, 5444.

[4]   Z. Zhang, M. N. Hedhili, H. Zhu, P. Wang, *Physical chemistry chemical physics: PCCP* **2013**, 15, 15637.

[5]   J. Zhi, W. Zhao, X. Liu, A. Chen, Z. Liu, F. Huang, *Advanced Functional Materials* **2014**, 24, 2013.

[6]   B. B. McKeon, J. Furukawa, S. Fenstermacher, *Proceedings of the IEEE* **2014**, 102, 951.

[7]   L.-R. Chen, S.-L. Wu, T.-R. Chen, presented at Sustainable Energy Technologies (ICSET), 2010 IEEE International Conference on **2010**.

[8]   H. Wang, Q. Hao, X. Yang, L. Lu, X. Wang, *Nanoscale* **2010**, 2, 2164.

[9]   Q. Wu, Y. Xu, Z. Yao, A. Liu, G. Shi, *ACS nano* **2010**, 4, 1963.